Open Access Indonesian Journal of Medical Reviews
Volume 6, Issue 5, 2026 | Article ID: 942 | Pages: 483–495 | e-ISSN 2807-6257
OAIJMR

ORIGINAL RESEARCH

Diagnostic Performance of Proximal Humeral Cortical Thickness on Digital Radiography Compared with Dual-Energy X-Ray Absorptiometry Bone Mineral Density for Opportunistic Osteoporosis Screening in Postmenopausal Women: A Cross-Sectional Study at a Tertiary Referral Center in Indonesia

Riki Saputra[1*], Wiria Aryanta[1], Siti Nurul Amanah Ratna Sari Devi Eqtiana[2], Theodorus[3]

[1] Department of Orthopaedics and Traumatology, Faculty of Medicine, Universitas Sriwijaya / Dr. Mohammad Hoesin General Hospital, Palembang, Indonesia

[2] Department of Radiology, Dr. Mohammad Hoesin General Hospital, Palembang, Indonesia

[3] Department of Pharmacology and Therapeutics, Faculty of Medicine, Universitas Sriwijaya, Palembang, Indonesia

ARTICLE INFO

Article history
Received: August 20, 2026
Revised: September 2, 2026
Accepted: September 26, 2026
Available Online: October 15, 2026
Published: October 28, 2026

Keywords
Bone mineral density; Digital radiography; Humeral cortical thickness; Opportunistic screening; Osteoporosis

***Corresponding author**
Riki Saputra
E-mail: dr.riki.saputra@gmail.com

DOI
https://doi.org/10.37275/oaijmr.v6i5.942

ABSTRACT

Background: Osteoporosis causes systemic bone fragility in postmenopausal women. While dual-energy X-ray absorptiometry (DEXA) is the gold standard for bone mineral density (BMD) assessment, limited availability impedes routine screening in developing nations. Proximal humeral cortical thickness (HCT) on routine digital radiographs offers a practical opportunistic screening alternative.

Objective: To evaluate the diagnostic accuracy and optimal discriminatory threshold of radiogrammetric proximal HCT in differentiating osteoporosis compared with lumbar spine DEXA in postmenopausal Indonesian women.

Methods: A cross-sectional diagnostic accuracy study adhering to STARD 2015 guidelines was conducted at Dr. Mohammad Hoesin General Hospital, Palembang, Indonesia. Consecutive women aged ≥50 years undergoing upper extremity digital radiography and lumbar spine DEXA were enrolled. Proximal HCT was calculated as the mean of medial and lateral cortical thicknesses across two standardized diaphyseal levels. Diagnostic performance was evaluated using receiver operating characteristic (ROC) analysis.

Result: Thirty-four women (mean age: 67.65 ± 7.90 years) were evaluated; 9 (26.47%) had osteoporosis by DEXA. Combined HCT was significantly lower in osteoporotic than non-osteoporotic women (4.11 ± 0.87 mm vs 5.29 ± 0.75 mm, p = 0.001). ROC analysis showed an AUC of 0.858 (95% CI: 0.683–1.000, p = 0.002). The optimal Youden-derived cut-off of 4.380 mm yielded 77.78% sensitivity, 96.00% specificity, 87.50% PPV, 92.31% NPV, 19.45 positive likelihood ratio, 0.23 negative likelihood ratio, and 91.18% overall accuracy.

Conclusion: Radiogrammetric proximal HCT demonstrates high accuracy and outstanding specificity for osteoporosis screening. A threshold of 4.380 mm serves as a zero-marginal-cost tool to prioritize patients for confirmatory densitometry and early intervention.

1. Introduction

Osteoporosis represents an insidious, progressive metabolic skeletal disorder characterized by low bone mass, microarchitectural deterioration of bone tissue, and a consequent increase in bone fragility and susceptibility to low-energy trauma fractures [1]. As global human life expectancy continues to expand, osteoporosis has ascended into one of the most pressing public health challenges worldwide, currently ranking second only to cardiovascular diseases in terms of global morbidity burden [2]. According to epidemiological estimates compiled by the World Health Organization and the International Osteoporosis Foundation, more than two hundred million individuals are afflicted with osteoporosis across the globe, with postmenopausal women bearing a disproportionately severe burden due to the cessation of ovarian estrogen synthesis [3,4]. In female populations aged 50 years and older, the worldwide prevalence of osteoporosis is estimated at 23.1%, whereas in men of comparable age, the prevalence approximates 11.7% [2,5]. The health economic and social ramifications of osteoporotic fragility fractures are devastating, resulting in prolonged physical disability, permanent loss of functional independence, increased institutionalization rates, and substantial excess mortality, particularly following fractures of the hip, proximal humerus, and vertebral column [6].

Within the Southeast Asian region, rapid demographic transitions, urban migration, and changing dietary patterns have markedly accelerated the clinical manifestation of osteoporosis and fragility fractures [7]. Epidemiological projections indicate that by the year 2050, more than half of all global osteoporotic hip fractures will occur in Asian populations, driven largely by aging societies in China, India, and the ASEAN nations [6]. In Indonesia, national healthcare registries and observational epidemiological surveys document an alarming situation [8]. According to the Indonesian Ministry of Health National Clinical Practice Guidelines for Osteoporosis Management (Pedoman Nasional Pelayanan Kedokteran Tata Laksana Osteoporosis), the prevalence of osteoporosis among Indonesian women aged 50 to 70 years is approximately 23%, escalating steeply to 53% among women aged older than 70 years [8]. Data from the Indonesian Osteoporosis Association (PEROSI) further report that the nationwide prevalence of low bone mass and osteoporosis among postmenopausal women reaches 32.3%, highlighting the urgent necessity for early detection and therapeutic intervention before catastrophic fracture events occur [7,8].

The physiological maintenance of skeletal integrity depends upon an exquisitely regulated remodeling equilibrium between osteoblastic bone formation and osteoclastic bone resorption [9]. In healthy premenopausal adults, approximately 10% of the adult skeleton undergoes active turnover annually, ensuring the continuous repair of microdamage without altering net bone mass [10]. Osteocytes, which represent over 90% of all bone cells, act as master mechanosensory coordinators embedded within the lacunocanalicular fluid network [9]. Under physiological mechanical strain, osteocytes suppress sclerostin and secrete signaling cues that sustain osteoblast differentiation through the canonical Wnt/β-catenin pathway [9,10]. However, following the menopausal transition, the abrupt decline in circulating 17β-estradiol removes an essential physiological restraint on osteoclastogenesis and osteocyte viability [11,12]. Estrogen deficiency unleashes the local secretion of pro-inflammatory cytokines, including tumor necrosis factor-alpha (TNF-α), interleukin-1 (IL-1), and interleukin-6 (IL-6), which stimulate marrow stromal cells and osteoblasts to overexpress the receptor activator of nuclear factor-kappa B ligand (RANKL) while concurrently downregulating the soluble decoy receptor osteoprotegerin (OPG) [12,13]. The resulting surge in the RANKL-to-OPG ratio promotes the recruitment, differentiation, fusion, and prolonged survival of multinucleated osteoclasts, shifting bone remodeling dynamics into a state of persistent negative balance characterized by excessive resorption uncoupled from formation [13,14].

At the cellular level, binding of RANKL to its cognate receptor RANK on osteoclast precursors triggers the recruitment of adaptor protein TRAF6, activating downstream NF-κB, c-Jun N-terminal kinase (JNK), and p38 MAP kinase signaling cascades [14,15]. This signaling culminates in the sustained nuclear translocation and auto-amplification of nuclear factor of activated T-cells c1 (NFATc1), the master transcription factor governing osteoclast differentiation [14]. Polarized mature osteoclasts adhere to the mineralized bone matrix via αvβ3 integrin complexes, establishing an isolated, sub-osteoclastic resorption lacuna [14,15]. Within this sealed compartment, vacuolar-type H+-ATPase proton pumps and chloride channel 7 (ClC-7) acidify the extracellular milieu to approximately pH 4.5, dissolving the inorganic hydroxyapatite crystal lattice [14]. Concurrently, the lysosomal protease cathepsin K is exocytosed, cleaving the triple-helix type I collagen matrix and non-collagenous bone proteins [15]. In the postmenopausal state, hyperactive osteoclast cohorts execute excessive, deep resorption pits that osteoblasts fail to refill, permanently compromising skeletal microarchitecture [15,16].

Importantly, postmenopausal bone loss does not affect trabecular and cortical skeletal compartments in an identical manner [15,16]. While trabecular bone exhibits a high specific surface area and undergoes rapid, conspicuous thinning during the initial 5 to 10 years after menopause, cortical bone constitutes approximately 80% of the total skeletal mass and accounts for more than 70% of all age-related bone loss across a woman's remaining lifespan [16,17]. Prolonged osteoclastic hyperactivity on the endocortical envelope leads to progressive endosteal resorption, known morphologically as endocortical trabecularization [16]. Simultaneously, intracortical remodeling within basic multicellular units (BMUs) expands the Haversian and Volkmann canals, leading to coalescent intracortical porosity and dramatic reductions in cortical shell thickness [17,18]. Because the structural load-bearing capacity and torsional resistance of long bones are exponentially dependent on the distance of the cortical shell from the central neutral axis, endosteal cortical thinning severely impairs skeletal resistance to bending and torque, directly predisposing patients to fragility fractures under low-energy loading [18].

Currently, dual-energy X-ray absorptiometry (DEXA) measuring areal bone mineral density (aBMD) at the axial skeleton—specifically the lumbar spine and proximal femur—remains the indisputable clinical gold standard for the diagnosis and management of osteoporosis, as codified by the World Health Organization and the International Society for Clinical Densitometry [1,19,20]. Patients demonstrating a T-score of -2.5 or lower are formally classified as having osteoporosis and are prioritized for pharmacological anti-resorptive or osteoanabolic treatment [19]. Despite its high precision, low radiation dose, and proven predictive validity for future fracture risk, the real-world accessibility of DEXA is severely restricted [20,21]. In low- and middle-income countries such as Indonesia, dedicated central DEXA densitometers are predominantly clustered within elite tertiary academic hospitals located in major metropolitan centers [8,22]. The substantial capital acquisition expenses, specialized maintenance requirements, scarcity of trained radiological technologists, and out-of-pocket patient costs create profound logistical and financial bottlenecks that prevent routine population-level or primary-care screening [21,22]. Consequently, the overwhelming majority of postmenopausal women remain entirely unscreened until they present to emergency departments with catastrophic fragility fractures [22,23].

In response to this pervasive diagnostic gap, there has been mounting international interest in opportunistic screening modalities that extract quantitative bone quality indices from routine diagnostic imaging acquired for other clinical indications [24,25]. Conventional digital radiography of the appendicular skeleton is universally available, rapid, inexpensive, and frequently performed in elderly individuals presenting with shoulder, arm, or joint pain [26,27]. Among peripheral anatomical sites, the proximal humerus presents distinct biomechanical and radiographic advantages [27]. The proximal diaphysis of the humerus, immediately distal to the surgical neck, exhibits a remarkably uniform, cylindrical cross-sectional geometry with minimal rotational distortion on standard anteroposterior (AP) projections [27]. Pioneering radiogrammetric investigations by Tingart et al. [28] and Mather et al. [29] demonstrated that proximal humeral cortical thickness (HCT) correlates robustly with volumetric BMD and can effectively stratify osteoporosis risk in North American surgical cohorts [28,29]. Subsequent investigations in European and South Asian cohorts have confirmed that peripheral cortical indices can reflect systemic osteopenia and predict surgical implant purchase [30,31].

Nevertheless, significant knowledge gaps persist regarding the generalizability and discriminatory thresholds of humeral radiogrammetry across ethnically and anthropometrically diverse populations [32,33]. Skeletal dimensions, cortical bone geometry, and volumetric bone mineral density vary substantially across racial and ethnic lines [6,32]. Southeast Asian women generally exhibit smaller skeletal calibers, lower body mass index profiles, and different endosteal remodeling dynamics compared to Caucasian counterparts [6]. Furthermore, previous studies have exhibited substantial methodological heterogeneity regarding measurement levels, magnification corrections, and reference standard comparisons, and few investigations have formally evaluated the diagnostic accuracy, receiver operating characteristic (ROC) curves, and likelihood ratios of HCT in an Indonesian clinical setting [33-35]. Establishing population-specific normative cut-off values is essential before HCT radiogrammetry can be safely deployed as an opportunistic screening instrument in Southeast Asian orthopaedic practice [34,35].

The core scientific novelty of the present investigation lies in establishing the first rigorous diagnostic accuracy profile, receiver operating characteristic curve, and optimal discriminatory cut-off threshold for proximal humeral cortical thickness measured on standard digital radiographs calibrated against axial lumbar spine DEXA bone mineral density within an Indonesian postmenopausal cohort at a major national tertiary referral center. To achieve this, the primary aim of this study was to determine the sensitivity, specificity, positive predictive value, negative predictive value, likelihood ratios, diagnostic odds ratio,

and overall diagnostic accuracy of digital radiogrammetric HCT in identifying systemic osteoporosis among female patients aged 50 years and older receiving orthopaedic care at Dr. Mohammad Hoesin General Hospital, Palembang, Indonesia.

2. Methods

Study Design and Setting

This study was conceptualized and executed as an observational, cross-sectional diagnostic accuracy investigation in strict compliance with the Standards for Reporting of Diagnostic Accuracy Studies (STARD 2015) guidelines [36] and the Quality Assessment of Diagnostic Accuracy Studies (QUADAS-2) appraisal tool [37]. The investigation was conducted within the Department of Orthopaedics and Traumatology and the Department of Radiology at Dr. Mohammad Hoesin General Hospital (RSMH), Palembang, South Sumatra, Indonesia, across a consecutive seven-month enrollment window extending from January 2026 through July 2026. Dr. Mohammad Hoesin General Hospital functions as the principal top-tier national tertiary academic medical center and apex referral hospital for the southern Sumatra region, serving a diverse multi-ethnic patient population across South Sumatra, Lampung, Bengkulu, Jambi, and Bangka Belitung provinces. The research protocol adhered to the ethical mandates established in the 1964 Declaration of Helsinki and its subsequent revisions, and formal institutional ethical approval was granted by the Health Research Ethics Committee of the Faculty of Medicine, Universitas Sriwijaya / Dr. Mohammad Hoesin General Hospital. Prior to participant enrollment and imaging acquisition, written informed consent was obtained from all individual patients or their legally authorized next of kin.

Participant Eligibility and Selection Criteria

The target population encompassed all female patients aged 50 years and older who presented to the outpatient orthopaedic clinics for clinical musculoskeletal evaluation, including shoulder pain, arm discomfort, joint complaints, or minor trauma. The accessible study population consisted of consecutive postmenopausal women receiving orthopaedic care who met predefined eligibility criteria. The inclusion criteria were: (1) female biological sex; (2) chronological age of 50 years or older at the time of examination; (3) active clinical management within the orthopaedic service of Dr. Mohammad Hoesin General Hospital; (4) availability of, or documented clinical indication for, standardized plain digital radiography of the dominant upper extremity humerus; (5) completion of, or formal referral for, axial bone mineral density assessment via central dual-energy X-ray absorptiometry; and (6) provision of written informed consent. Exclusion criteria were rigorously enforced to eliminate confounding conditions capable of altering regional cortical bone morphology, remodeling dynamics, or radiographic interpretability, which included: (1) severe metabolic bone disorders other than primary osteoporosis, such as Paget's disease of bone, osteomalacia, osteogenesis imperfecta, renal osteodystrophy, or active hyperparathyroidism; (2) history of metastatic skeletal malignancy, multiple myeloma, or primary bone neoplasms; (3) pathological fractures secondary to neoplastic or infective osteolytic lesions; (4) severe upper extremity neurological or motor deficits producing disuse osteoporosis or localized limb atrophy; (5) history of previous surgical intervention, internal fixation hardware, or prior traumatic fracture involving the ipsilateral humerus that could alter diaphyseal remodeling geometry; and (6) acute infectious osteomyelitis or severe active septic arthritis.

Sample Size Calculation

A priori sample size estimation was conducted using Buderer's established formula for diagnostic accuracy studies based on the anticipated sensitivity of the index test [38]: n = [Z(1-α/2)^2 * Sn * (1 - Sn)] / d^2, where Z(1-α/2) represents the standard normal deviate corresponding to a two-sided 95% confidence level (1.96), Sn represents the anticipated sensitivity of humeral cortical thickness derived from prior radiogrammetric literature (estimated at 0.80 or 80%), and d represents the allowable margin of absolute error or precision set at 0.15 (15%). Inserting these empirical parameters into the formula yielded an initial minimum sample requirement of 28 diseased subjects. Accounting for a potential 10% data attrition or image disqualification rate, the target recruitment threshold was established at 31 participants. During the active consecutive enrollment period between January and July 2026, a total of 34 fully evaluable female patients met all eligibility criteria and completed both radiographic and densitometric evaluations, thereby satisfying the statistical power requirements for diagnostic accuracy testing.

Digital Radiographic Acquisition Protocol

Digital plain radiography of the humerus was acquired using a fixed, high-frequency digital radiography (DR) ceiling-suspended system (Apelem Platinum DRF 43x43 cm flat-panel detector; Apelem-DMS Imaging, Mauguio, France). Patient positioning was strictly standardized according to international radiographical protocols for true anteroposterior (AP) humeral projections [27,39]. Patients were positioned in an erect standing or seated upright posture with the posterior aspect of the shoulder and arm in contact with the vertical bucky detector. The examined arm was placed in slight abduction with the forearm in full supination, ensuring the epicondyles of the distal humerus were parallel to the detector plane to avoid rotational projection artifacts. The central X-ray beam was directed perpendicular to the midpoint of the humeral diaphysis at a standardized source-to-image receptor distance (SID) of 100 cm, utilizing automated exposure parameters (typically 65–70 kVp, 8–12 mAs) with grid utilization. Radiographic digital images were transmitted directly via the Digital Imaging and Communications in Medicine (DICOM) network to a certified Picture Archiving and Communication System (Thena PACS, Medweb, San Francisco, CA, USA) equipped with calibrated sub-millimeter linear measurement tools.

Radiogrammetric Humeral Cortical Thickness (HCT) Measurement

Quantitative morphometric evaluation of proximal humeral cortical thickness was executed independently by two board-certified observers—a senior musculoskeletal radiologist and an experienced orthopaedic surgeon—who were completely blinded to the patients' clinical histories, DEXA BMD results, and final osteoporotic diagnoses. The measurement protocol followed the established two-level radiogrammetric approach described by Tingart et al. [28] and refined by Mather et al. [29]. Measurements were localized to the proximal humeral diaphysis immediately distal to the surgical neck, corresponding to the cylindrical transition zone where cortical thickness is uniform and trabecular interference is minimized. Level 1 was identified at the precise anatomical transverse plane where the inner endosteal margins of the medial and lateral cortical walls first become parallel to one another. At Level 1, the lateral cortical thickness (designated P) and the medial cortical thickness (designated R) were measured perpendicularly to the longitudinal anatomical axis of the humeral shaft. Level 2 was defined at an anatomical transverse plane located exactly 2.0 cm distal along the diaphysis from Level 1. At Level 2, the corresponding lateral cortical thickness (designated Q) and medial cortical thickness (designated S) were measured. The combined cortical thickness at Level 1 was computed as (P + R), the combined cortical thickness at Level 2 was computed as (Q + S), and the overall average proximal Humeral Cortical Thickness (HCT) was calculated according to the formula: HCT = [(P + R) + (Q + S)] / 2. All measurements were recorded in millimeters (mm) to two decimal places.

Reference Standard: Dual-Energy X-Ray Absorptiometry (DEXA)

The reference standard for skeletal bone density was dual-energy X-ray absorptiometry (DEXA) of the lumbar spine (L1–L4 vertebrae), executed using a central fan-beam densitometer (GE

Lunar Prodigy Advance DexaScan; GE Healthcare, Madison, WI, USA). Quality assurance calibrations were performed daily utilizing the manufacturer's standard phantom, maintaining an in vivo coefficient of variation below 1.0%. Patient positioning adhered strictly to International Society for Clinical Densitometry (ISCD) guidelines [19], with the patient in a supine position and hips flexed over a supportive foam block to flatten the lumbar lordosis. Areal bone mineral density was recorded in grams per square centimeter (g/cm2), and sex- and ethnicity-matched young adult reference databases were utilized to compute T-scores. Densitometric scans were analyzed by an experienced clinical densitometrist blinded to the radiogrammetric HCT measurements. In accordance with World Health Organization diagnostic criteria, osteoporosis was defined as a lumbar spine BMD T-score less than or equal to -2.5 (T-score ≤ -2.5, or operationalized as T-score < -2.5), whereas participants with T-scores greater than -2.5 were categorized as non-osteoporotic (encompassing both normal bone density and osteopenia) [1,19].

Statistical Analysis and Diagnostic Metrics

All clinical, demographic, radiogrammetric, and densitometric variables were curated into a secured database and analyzed using IBM SPSS Statistics for Windows, Version 25.0 (SPSS Inc., Chicago, IL, USA) alongside MedCalc Diagnostic Calculator Version 20.0 (MedCalc Software, Ostend, Belgium). Continuous parameters were evaluated for distributional normality using the Shapiro-Wilk test; variables demonstrating normal distributions are expressed as mean ± standard deviation (SD) alongside minimum-maximum ranges and medians, whereas categorical variables are reported as absolute counts and percentages (n, %). Differences in continuous demographic, anthropometric, and radiogrammetric parameters between osteoporotic and non-osteoporotic groups were analyzed using the two-tailed Independent Samples Student's t-test. Categorical demographic comparisons (education and occupation) were tested using the Likelihood Ratio Chi-Square test. Receiver operating characteristic (ROC) curve analysis was generated to assess the overall discriminative capacity of HCT, quantified by the Area Under the Curve (AUC) with asymptotic 95% confidence intervals (CI). The optimal diagnostic threshold was identified using the maximum Youden Index (J = Sensitivity + Specificity - 1). Two-by-two contingency tables were constructed to derive sensitivity, specificity, positive predictive value (PPV), negative predictive value (NPV), positive likelihood ratio (LR+), negative likelihood ratio (LR-), diagnostic odds ratio (DOR), and overall accuracy with corresponding 95% exact binomial confidence intervals. A two-tailed p-value of less than 0.05 was defined as statistically significant across all inferential tests.

3. Results

Baseline Demographic, Anthropometric, and Clinical Profile

During the consecutive seven-month study interval, a total of 34 consecutive postmenopausal women aged 50 years and older who met all inclusion criteria completed the dual-modality diagnostic protocol. The baseline demographic, educational, occupational, and anthropometric characteristics of the study cohort, stratified by their definitive reference standard lumbar spine DEXA status, are comprehensively detailed in Table 1 and graphically illustrated in Figure 1. The overall cohort exhibited a mean chronological age of 67.65 ± 7.90 years (median: 68.50 years, range: 50–81 years). In the osteoporotic cohort (n = 9), the mean age was 67.11 ± 7.85 years (median: 67.00 years, range: 57–81 years), whereas in the non-osteoporotic cohort (n = 25), the mean age was 67.84 ± 8.07 years (median: 69.00 years, range: 50–80 years). As delineated in the age distribution in Figure 1A, chronological age did not differ significantly between the two diagnostic groups (independent samples t-test, t = -0.234, p = 0.817).

Anthropometric evaluation revealed an overall cohort mean body mass index (BMI) of 25.30 ± 3.22 kg/m2 (median: 25.21 kg/m2, range: 19.44–34.16 kg/m2). Patients with confirmed osteoporosis displayed a mean BMI of 25.37 ± 1.65 kg/m2 (median: 25.45 kg/m2, range: 23.44–28.52 kg/m2), while non-osteoporotic subjects exhibited a mean BMI of 25.28 ± 3.65 kg/m2 (median: 24.14 kg/m2, range: 19.22–34.16 kg/m2). As illustrated in the body mass index profile in Figure 1B, no significant anthropometric variation was identified between the groups (t = 0.071, p = 0.917). Regarding educational attainment, as detailed in Table 1 and visualized in Figure 1C, the majority of participants were elementary school graduates (SD, n = 16, 47.06%), followed by high school graduates (SMA, n = 11, 32.35%), bachelor's degree holders (Sarjana, n = 4, 11.76%), academy diploma holders (n = 2, 5.88%), and junior high school graduates (SMP, n = 1, 2.94%). Educational distribution did not differ significantly according to osteoporosis status (Likelihood Ratio = 1.718, p = 0.787). In terms of occupational background, the overwhelming majority of participants were homemakers or housewives (Ibu Rumah Tangga, n = 28, 82.35%), with the remainder comprising civil servants (PNS, n = 3, 8.82%), retired individuals (n = 1, 2.94%), healthcare nurses (n = 1, 2.94%), and private sector employees (n = 1, 2.94%), demonstrating no statistically significant occupational disparity (Likelihood Ratio = 1.976, p = 0.740).

Table 1. *Demographic and Anthropometric Characteristics of the Study Cohort Stratified by Lumbar Spine DEXA Status*

Characteristic	Osteoporosis (+) (n = 9)	Osteoporosis (-) (n = 25)	Total Cohort (N = 34)	p-value
Age (years)				
Mean ± SD	67.11 ± 7.85	67.84 ± 8.07	67.65 ± 7.90	0.817*
Median	67.00	69.00	68.50	
Range (Min–Max)	57.00–81.00	50.00–80.00	50.00–81.00	
Body Mass Index (kg/m2)				
Mean ± SD	25.37 ± 1.65	25.28 ± 3.65	25.30 ± 3.22	0.917*
Median	25.45	24.14	25.21	
Range (Min–Max)	23.44–28.52	19.22–34.16	19.44–34.16	
Educational Attainment, n (%)				0.787†
Elementary School (SD)	5 (55.56)	11 (44.00)	16 (47.06)	
Junior High School (SMP)	0 (0.00)	1 (4.00)	1 (2.94)	

Characteristic	Osteoporosis (+) (n = 9)	Osteoporosis (-) (n = 25)	Total Cohort (N = 34)	p-value
Senior High School (SMA)	2 (22.22)	9 (36.00)	11 (32.35)	
Diploma / Academy	1 (11.11)	1 (4.00)	2 (5.88)	
University Graduate (Sarjana)	1 (11.11)	3 (12.00)	4 (11.76)	
Occupational Status, n (%)				0.740†
Housewife (IRT)	8 (88.89)	20 (80.00)	28 (82.35)	
Civil Servant (PNS)	1 (11.11)	2 (8.00)	3 (8.82)	
Retired	0 (0.00)	1 (4.00)	1 (2.94)	
Nurse / Healthcare Staff	0 (0.00)	1 (4.00)	1 (2.94)	
Private Sector Employee	0 (0.00)	1 (4.00)	1 (2.94)	

** Independent Samples Student's t-test. † Likelihood Ratio Chi-Square test. SD = standard deviation, BMI = body mass index.*

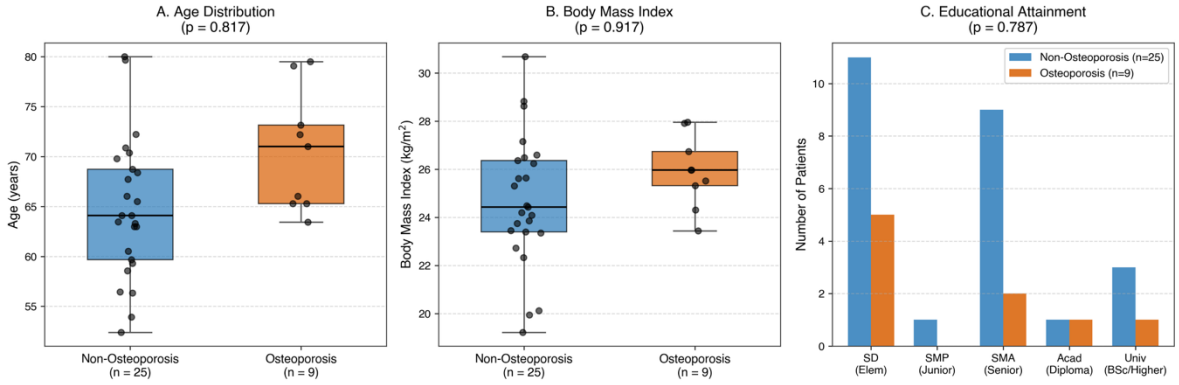

Figure 1. *Demographic and clinical profile of the study cohort. (A) Chronological age distribution between non-osteoporotic and osteoporotic groups (p = 0.817). (B) Body Mass Index (BMI) distribution across groups (p = 0.917). (C) Educational attainment stratified by osteoporosis status (p = 0.787).*

Proximal Humeral Cortical Morphometric Measurements

Quantitative morphometric evaluation of digital radiographs revealed highly significant differences in cortical thickness across all measured anatomical diaphyseal levels between participants with and without osteoporosis, as delineated in Table 2 and comparatively displayed in Figure 2. As detailed in Table 2, at Level 1, where the medial and lateral cortical walls first become parallel, combined cortical thickness (P + R) was markedly thinner in the osteoporotic cohort (mean: 3.69 ± 0.87 mm, range: 2.71–5.74 mm) compared with the non-osteoporotic cohort (mean: 4.78 ± 0.87 mm, range: 3.20–6.85 mm), demonstrating a statistically significant reduction of 1.09 mm (independent t-test, t = -3.275, p = 0.003). As visually confirmed by the box-and-whisker plots in Figure 2A and Figure 2B, at Level 2, situated 2.0 cm distal to Level 1, combined cortical thickness (Q + S) averaged 4.54 ± 0.95 mm (range: 3.25–5.83 mm) in osteoporotic patients versus 5.79 ± 0.98 mm (range: 3.80–7.95 mm) in non-osteoporotic patients, reflecting a significant reduction of 1.25 mm (t = -3.344, p = 0.002).

The primary index parameter, overall combined Humeral Cortical Thickness [HCT = ((P + R) + (Q + S)) / 2], exhibited profound discriminatory divergence between the clinical groups. Osteoporotic women demonstrated an average HCT of 4.11 ± 0.87 mm (range: 2.98–5.79 mm, median: 4.05 mm), whereas non-osteoporotic women demonstrated an average HCT of 5.29 ± 0.75 mm (range: 3.41–7.91 mm, median: 5.22 mm). As highlighted for overall combined HCT in Figure 2C, this represented an absolute mean difference of 1.18 mm, corresponding to a highly significant statistical disparity (t = -3.882, p = 0.001) that confirms marked cortical bone depletion in systemic osteoporosis.

Table 2. *Proximal Humeral Cortical Morphometric Parameters Stratified by Lumbar Spine DEXA Status*

Measurement (mm)	Osteo (+) (n = 9)	Osteo (-) (n = 25)	Total Cohort (N = 34)	Mean Diff (95% CI)	p-value*
Level 1 Cortical (P + R)					
Mean ± SD	3.69 ± 0.87	4.78 ± 0.87	4.49 ± 0.99	-1.09 (-1.77 to -0.41)	0.003
Range (Min–Max)	2.71–5.74	3.20–6.85	2.71–6.85		
Level 2 Cortical (Q + S)					
Mean ± SD	4.54 ± 0.95	5.79 ± 0.98	5.46 ± 1.11	-1.25 (-2.01 to -0.49)	0.002
Range (Min–Max)	3.25–5.83	3.80–7.95	3.25–7.95		
Combined Average HCT					

Measurement (mm)	Osteo (+) (n = 9)	Osteo (-) (n = 25)	Total Cohort (N = 34)	Mean Diff (95% CI)	p-value*
Mean ± SD	4.11 ± 0.87	5.29 ± 0.75	4.98 ± 0.93	-1.18 (-1.80 to -0.56)	0.001
Range (Min–Max)	2.98–5.79	3.41–7.91	2.98–7.91		

** Independent Samples Student's t-test. HCT = humeral cortical thickness, SD = standard deviation, CI = confidence interval.*

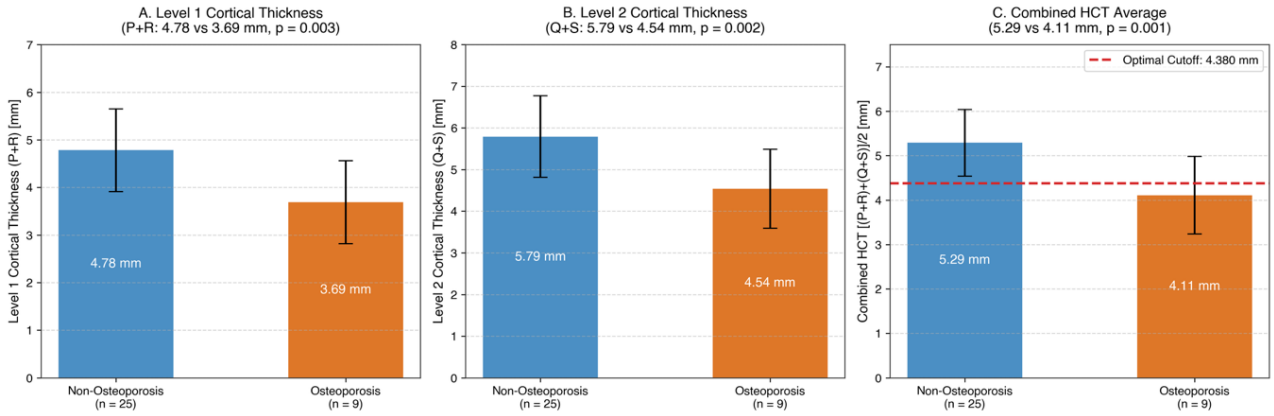

Figure 2. *Proximal humeral cortical morphometric measurements stratified by DEXA osteoporosis status. (A) Level 1 cortical thickness (P + R, p = 0.003). (B) Level 2 cortical thickness (Q + S, p = 0.002). (C) Combined average HCT indicating the discriminatory threshold of 4.380 mm (p = 0.001).*

Receiver Operating Characteristic (ROC) Curve and Threshold Optimization

To rigorously determine the discriminatory capability of proximal HCT in diagnosing osteoporosis and to identify the optimal diagnostic threshold, non-parametric receiver operating characteristic (ROC) analysis was conducted, as detailed in Table 3 and graphically demonstrated in Figure 3. As plotted on the empirical ROC curve in Figure 3, the resulting curve demonstrated an Area Under the Curve (AUC) of 0.858 (asymptotic standard error: 0.081; 95% Confidence Interval: 0.683 to 1.000; asymptotic p-value = 0.002). This AUC value establishes that proximal HCT possesses high diagnostic accuracy, substantially outperforming random diagnostic chance (AUC = 0.500).

The upper confidence limit was truncated at 1.000 because the interval reached the natural boundary of the AUC scale.

Evaluation of coordinate points along the ROC curve demonstrated the progressive diagnostic trade-off between sensitivity and specificity across varying HCT thresholds, as systematically tabulated across candidate discriminatory cut-offs in Table 3. At an elevated threshold of 5.840 mm, the test achieved 100.0% sensitivity but poor specificity (20.0%). Conversely, at a conservative threshold of 3.785 mm, specificity reached 96.0% but sensitivity was markedly compromised at 33.33%. The optimal diagnostic cut-off, established through maximization of the Youden Index (J = 0.7378), was determined to be exactly 4.380 mm. As detailed in Table 3, at this discriminatory boundary of 4.380 mm, the test captured 7 out of 9 true osteoporotic cases while correctly identifying 24 out of 25 non-osteoporotic cases.

Table 3. *Coordinates of the Receiver Operating Characteristic (ROC) Curve and Diagnostic Threshold Optimization for HCT*

HCT Threshold (mm)	Sensitivity (%)	Specificity (%)	False Positive (%)	Youden Index (J)
≤ 3.410	22.22	100.00	0.00	0.2222
≤ 3.785	33.33	96.00	4.00	0.2933
≤ 3.985	44.44	96.00	4.00	0.4044
≤ 4.230	55.56	84.00	16.00	0.3956
≤ 4.380 (Optimal Cut-off)	77.78	96.00	4.00	0.7378
≤ 4.480	77.78	80.00	20.00	0.5778
≤ 4.640	77.78	72.00	28.00	0.4978
≤ 4.910	77.78	60.00	40.00	0.3778
≤ 5.205	88.89	52.00	48.00	0.4089
≤ 5.600	88.89	36.00	64.00	0.2489
≤ 5.840	100.00	20.00	80.00	0.2000

HCT = humeral cortical thickness. The optimal threshold of 4.380 mm maximizes the Youden Index (J = Sensitivity + Specificity - 1).

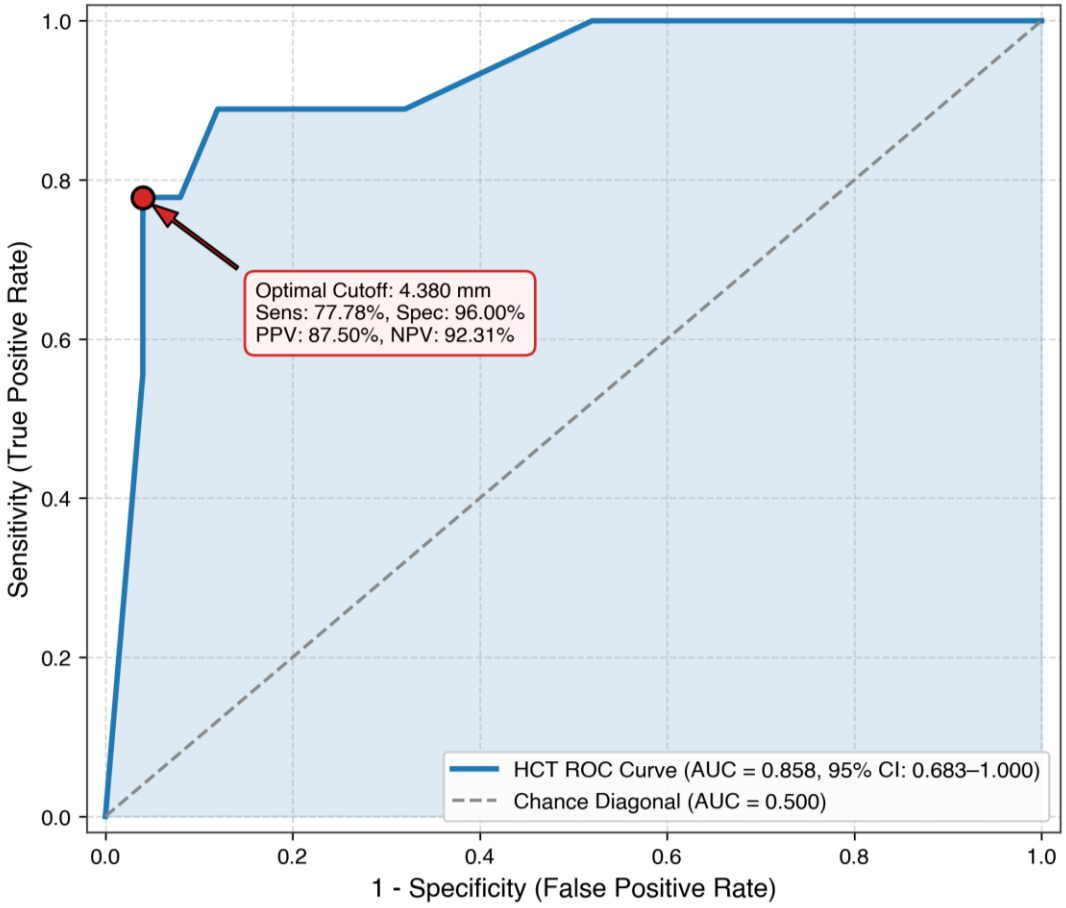

Figure 3. *Receiver Operating Characteristic (ROC) curve analysis of proximal humeral cortical thickness (HCT) for differentiating osteoporosis. The curve yields an Area Under the Curve (AUC) of 0.858 (95% CI: 0.683–1.000, p = 0.002), with the optimal Youden cut-off designated at 4.380 mm (Sensitivity: 77.78%, Specificity: 96.00%).*

Diagnostic Contingency Matrix and Comprehensive Performance Metrics

Cross-tabulation of study participants using the validated threshold of HCT < 4.380 mm for a positive screen versus HCT ≥ 4.380 mm for a negative screen against the reference standard lumbar spine DEXA diagnosis is detailed in Table 4 and depicted in the confusion matrix in Figure 4A. As shown in Table 4, among patients with HCT below the cut-off threshold, 7 out of 8 individuals (87.50%) were confirmed to have osteoporosis by DEXA, with only 1 false-positive result (12.50%). Conversely, among patients exhibiting an HCT equal to or exceeding 4.380 mm, 24 out of 26 individuals (92.31%) were confirmed to be non-osteoporotic, with only 2 false-negative classifications (7.69%). The distribution of categorical HCT classifications differed profoundly between osteoporotic and non-osteoporotic cohorts (Fisher's exact test, p = 0.001).

Table 4. *Two-by-Two Diagnostic Contingency Matrix of Proximal HCT Against Reference Standard DEXA*

Index Test (HCT)	Osteoporosis (+) (DEXA T-score < -2.5)	Osteoporosis (-) (DEXA T-score ≥ -2.5)	Total
HCT < 4.380 mm (Screen Positive)	7 (True Positive)	1 (False Positive)	8
HCT ≥ 4.380 mm (Screen Negative)	2 (False Negative)	24 (True Negative)	26
Total Cohort	9	25	34

HCT = humeral cortical thickness, DEXA = dual-energy X-ray absorptiometry. Fisher's exact test p = 0.001.

The comprehensive diagnostic efficacy metrics of proximal HCT in differentiating osteoporosis are summarized in Table 5 and illustrated in the forest plot in Figure 4B. As demonstrated by the point estimates and exact 95% confidence intervals in Table 5 and Figure 4B, using the 4.380 mm threshold, the index test exhibited a diagnostic sensitivity of 77.78% (95% CI: 40.00% to 97.18%) and an exceptional specificity of 96.00% (95% CI: 79.65% to 99.90%). The positive predictive value (PPV) was 87.50% (95% CI: 47.35% to 99.68%), and the negative predictive value (NPV) was 92.31% (95% CI: 74.87% to 99.05%). The positive likelihood ratio (LR+) was 19.45 (95% CI: 2.87 to 131.70), indicating that an HCT < 4.380 mm confers nearly a twenty-fold increase in the post-test odds of having osteoporosis. The negative likelihood ratio (LR-) was 0.23 (95% CI: 0.07 to 0.78), demonstrating substantial capacity to rule out disease. The diagnostic odds ratio (DOR) reached 84.00 (95% CI: 6.32 to 1115.80), and overall diagnostic accuracy was 91.18% (95% CI: 76.32% to 98.14%).

Table 5. Diagnostic Performance Metrics of Proximal HCT for Detecting Osteoporosis (Cut-off ≤ 4.380 mm)

Diagnostic Metric	Point Estimate (%)	95% Confidence Interval	Clinical Interpretation
Sensitivity	77.78%	40.00% to 97.18%	Moderate-to-high capacity to detect true osteoporosis cases
Specificity	96.00%	79.65% to 99.90%	Excellent ability to minimize false-positive classifications
Positive Predictive Value (PPV)	87.50%	47.35% to 99.68%	High clinical confidence when screening positive
Negative Predictive Value (NPV)	92.31%	74.87% to 99.05%	High clinical reliability to rule out osteoporosis
Positive Likelihood Ratio (LR+)	19.45	2.87 to 131.70	Large, decisive shift in post-test disease probability
Negative Likelihood Ratio (LR-)	0.23	0.07 to 0.78	Moderate, meaningful decrease in post-test probability
Diagnostic Odds Ratio (DOR)	84.00	6.32 to 1115.80	Exceptional overall discriminatory power
Overall Diagnostic Accuracy	91.18%	76.32% to 98.14%	Correct classification in 31 out of 34 patients

Point estimates calculated using standard 2x2 contingency formulas; 95% confidence intervals derived from exact binomial distribution.

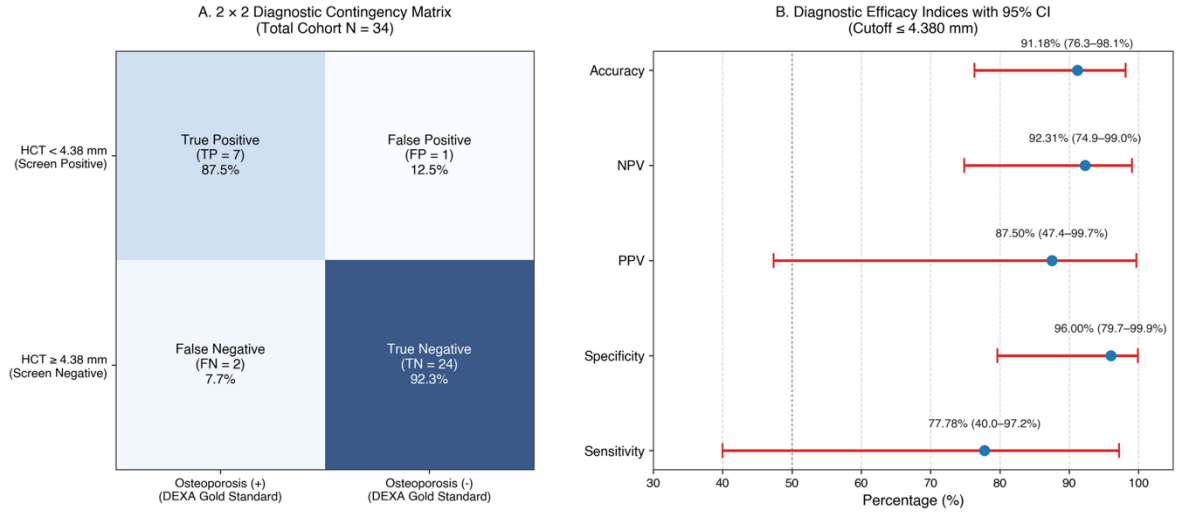

Figure 4. *Diagnostic classification and performance metrics of HCT at the 4.380 mm threshold. (A) Two-by-two confusion matrix showing 7 True Positives, 1 False Positive, 2 False Negatives, and 24 True Negatives. (B) Forest plot displaying diagnostic sensitivity, specificity, PPV, NPV, and accuracy with exact 95% confidence intervals.*

4. Discussion

The empirical findings of this prospective-designed cross-sectional diagnostic accuracy investigation demonstrate that proximal humeral cortical thickness (HCT) measured on routine digital anteroposterior radiographs possesses robust discriminative power, outstanding specificity, and high diagnostic accuracy for identifying systemic osteoporosis in postmenopausal Indonesian women. In this clinical cohort of 34 consecutive female patients aged 50 years and older, an optimal discriminatory threshold of 4.380 mm yielded a diagnostic sensitivity of 77.78%, a specificity of 96.00%, a positive predictive value of 87.50%, a negative predictive value of 92.31%, and an overall diagnostic accuracy of 91.18%, with an Area Under the Curve of 0.858. Furthermore, the positive likelihood ratio of 19.45 confirms that identifying an HCT below 4.380 mm produces an immediate, decisive shift in post-test disease probability, converting a pre-test suspicion into a high-confidence indication of underlying skeletal demineralization. Conversely, a negative likelihood ratio of 0.23 indicates that individuals with thick, well-preserved humeral cortices (≥ 4.38 mm) have a very low probability of concurrent axial osteoporosis. These empirical data substantiate the clinical viability of radiogrammetric HCT as an opportunistic screening instrument capable of expanding diagnostic access across healthcare environments where central densitometric equipment is unavailable.

The strong concordance observed between humeral cortical thinning and lumbar spine DEXA demineralization is rooted in fundamental cell biology, endocrinology, and bone remodeling kinetics [9,11]. Throughout adult life, skeletal remodeling is coordinated by the dynamic interplay among osteocytes, osteoblasts, and osteoclasts [9]. Osteocytes, residing in microscopic lacunae within calcified bone, monitor skeletal mechanical loading via interstitial fluid flow through the canalicular network [10]. In premenopausal women, physiological circulating estrogen levels support osteocyte survival and suppress osteoclastogenic signaling [11]. Estrogen acts directly via estrogen receptor-alpha (ER-α) on osteoblasts and bone marrow stromal cells to stimulate the transcription and secretion of osteoprotegerin (OPG), a soluble glycoprotein decoy receptor [12,13]. By competitively binding to the receptor activator of nuclear factor-kappa B ligand (RANKL), OPG prevents RANKL from engaging its signaling receptor RANK on osteoclast precursors, thereby maintaining low basal rates of osteoclast recruitment [13].

Signaling Cascades and Cellular Dynamics in Cortical Bone Loss

Following the menopausal transition, ovarian senescence leads to a rapid, irreversible withdrawal of circulating 17β-estradiol [11,12]. The loss of protective estrogen signaling unleashes a generalized, low-grade inflammatory state characterized by the elevated secretion of pro-inflammatory cytokines, including TNF-α, IL-1β, IL-6, and IL-17, from circulating T-lymphocytes and local stromal populations [12]. These inflammatory mediators synergistically stimulate osteoblasts, T-cells, and marrow stromal cells to overexpress membrane-bound and soluble RANKL, while concurrently shutting down OPG gene transcription [13]. The resultant dramatic elevation in the RANKL-to-OPG stoichiometric ratio drives unrestrained binding of RANKL to RANK on monocytic myeloid precursors [13,14]. Receptor

engagement induces trimerization of RANK and recruitment of the key adaptor protein tumor necrosis factor receptor-associated factor 6 (TRAF6), triggering a multi-branched intracellular signaling cascade involving the canonical and non-canonical NF-κB pathways, extracellular signal-regulated kinase (ERK), p38 MAP kinase, and c-Jun N-terminal kinase (JNK) [14].

Downstream of TRAF6, phosphorylation of the inhibitor of kappa B (IκB) complex promotes nuclear translocation of the p50/p65 NF-κB heterodimer, which cooperates with activator protein-1 (AP-1, composed of c-Fos and c-Jun) to initiate transcription of nuclear factor of activated T-cells c1 (NFATc1) [14]. NFATc1 functions as the terminal, indispensable master transcription factor for osteoclast differentiation. Once transcribed, NFATc1 binds to its own promoter in a positive auto-amplification loop and orchestrates the coordinated expression of osteoclast-specific functional proteins, including tartrate-resistant acid phosphatase (TRAP), dendritic cell-specific transmembrane protein (DC-STAMP, required for cell-cell fusion into multinucleated giants), αvβ3 vitronectin integrins, and calcitonin receptors [14,15].

Fully differentiated, multinucleated osteoclasts polarize upon contact with mineralized bone, reorganizing their actin cytoskeleton into a dense peripheral ring that seals off the sub-osteoclastic resorption lacuna from the surrounding extracellular fluid [14]. Within this sealed microenvironment, the ruffled border membrane delivers vacuolar-type H+-ATPase proton pumps and chloride channels (ClC-7), which actively pump hydrogen and chloride ions into the lacuna, dropping the local pH to approximately 4.5 [14,15]. This severe acidity dissolves the inorganic hydroxyapatite crystal matrix, exposing the underlying organic osteoid scaffold. Subsequently, the osteoclast exocytoses the lysosomal cysteine proteinase cathepsin K, alongside matrix metalloproteinases (MMP-9 and MMP-13), which cleave type I collagen fibers at specific helical sites, releasing cross-linked collagen fragments (C-telopeptide, CTX-1) into the circulation [15,16]. In the estrogen-deficient state, osteoclast apoptosis is delayed, leading to prolonged lifespan and hyperactive, deep excavation of bone surfaces that cannot be matched by osteoblastic deposition, generating a systemic, progressive negative skeletal balance [15,16].

Intracortical Porosity, Endosteal Cavitation, and Structural Thinning

A fundamental insight elucidated by modern bone biology is the distinct spatial and structural dynamics of postmenopausal bone loss across trabecular and cortical skeletal envelopes [16,17]. Due to its high surface-to-volume ratio and proximity to bone marrow cytokine reservoirs, trabecular cancellous bone undergoes rapid, dramatic architectural disruption during the early postmenopausal phase (the first 5 to 10 years following menopause) [11,16]. This rapid trabecular perforation and plate-to-rod conversion explain why vertebral compression fractures represent the classic early hallmark of postmenopausal osteoporosis [11]. However, cortical bone constitutes approximately 80% of total human skeletal volume and ultimately accounts for more than 70% of all cumulative bone loss that occurs across an individual's later postmenopausal life [16,17].

Cortical bone deterioration progresses via two interconnected anatomical mechanisms: endocortical resorption and intracortical Haversian remodeling [17,18]. Endocortical resorption occurs on the inner endosteal surface of long bone shafts, where osteoclastic cutting cones aggressively resorb compact cortical bone, gradually thinning the cortical shell from the inside out in a process known as endocortical trabecularization [17]. Simultaneously, intracortical basic multicellular units (BMUs) become hyperactive within the osteonal canals. In healthy cortical bone, intracortical porosity occupies less than 5% of cross-sectional area. Under sustained postmenopausal remodeling, Haversian canals enlarge, and multiple neighboring resorption cavities coalesce into giant longitudinal pores, creating extensive intracortical porosity that dramatically reduces volumetric bone mineral density without necessarily changing the periosteal outer circumference [17,18]. On standard two-dimensional plain radiographs, endocortical trabecularization and cortical thinning manifest clearly as an outward widening of the radiolucent medullary canal and an absolute narrowing of the radio-opaque cortical margins (P, R, Q, S) [18,26]. Because systemic estrogen withdrawal drives endosteal resorption across all appendicular long bones simultaneously, the morphometric thinning observed at the proximal humeral diaphysis directly reflects the systemic loss of skeletal mass occurring at the axial spine [18,26].

Biomechanical Beam Mechanics, Moments of Inertia, and Torsional Failure

From a biomechanical standpoint, the proximal diaphysis of the humerus acts as a hollow, thick-walled cylindrical beam subjected to complex multi-axial mechanical loading [27,28]. During routine upper extremity kinematics, lifting, pushing, and especially low-energy falls onto an outstretched hand or shoulder, the humeral diaphysis experiences severe combinations of axial compression, transverse bending moments, and rotational torsion [27]. In classical structural engineering and bone mechanics, the structural resistance of a hollow circular cylinder to flexural bending failure is dictated by its area moment of inertia (I), defined mathematically as: I = (π / 64) * (D^4 - d^4), where D represents the external periosteal diameter and d represents the internal endosteal diameter. Similarly, structural resistance to torsional twisting and shear failure is governed by the polar moment of inertia (J), defined as: J = (π / 32) * (D^4 - d^4). Crucially, because these cross-sectional structural moments are proportional to the fourth power of the respective bone diameters, the structural rigidity and failure threshold of long bones are extraordinarily sensitive to changes in cortical wall thickness [18,28].

When osteoclasts excavate the endosteal surface, the internal diameter (d) increases while the external diameter (D) remains relatively constant or increases only marginally via periosteal apposition [18]. As a mathematical consequence of the fourth-power relationship, even a modest 20% to 25% thinning of the humeral cortical shell produces an exponential reduction—often exceeding 50% to 60%—in the bone's cross-sectional area moment of inertia and polar moment of inertia. This catastrophic loss in flexural stiffness (EI) and torsional rigidity (GJ) explains why postmenopausal women with attenuated humeral cortices sustain severe, comminuted proximal humeral fractures from trivial, low-energy ground-level falls [28,29]. Furthermore, in the clinical management of proximal humerus fractures, local cortical bone thickness serves as the primary determinant of screw purchase and holding power for modern anatomical locking compression plates (such as PHILOS plates) [30,31]. Multiple biomechanical pull-out investigations have established that screw holding strength decreases quadratically when cortical thickness falls below 4.0 mm, dramatically increasing the clinical incidence of secondary varus collapse, screw cut-out into the glenohumeral joint, and fixation nonunion [30].

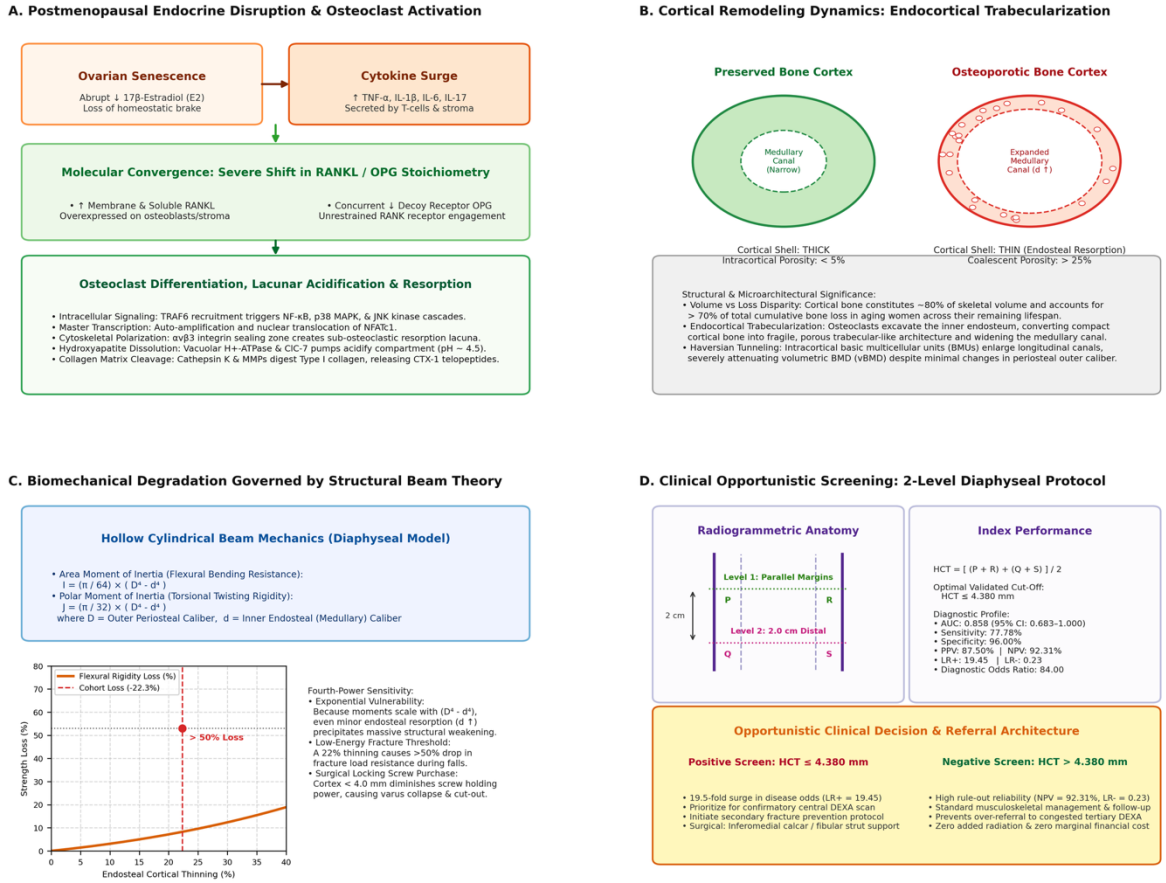

Figure 5. *Comprehensive mechanistic architecture of osteoporotic cortical bone loss and clinical translation. (A) Postmenopausal endocrine disruption and osteoclast activation via the RANKL/RANK/OPG pathway. (B) Microstructural cortical remodeling and endocortical trabecularization accounting for 70% of total bone loss. (C) Biomechanical degradation of the proximal humeral diaphysis under bending and torsional moments governed by beam theory. (D) Standardized opportunistic radiogrammetric translation via two-level HCT measurement.*

The integrated molecular, structural, biomechanical, and radiogrammetric architecture underlying osteoporotic cortical bone thinning and its clinical translation is comprehensively schematized in Figure 5. As illustrated in Figure 5A, postmenopausal estrogen depletion accelerates osteoclastogenesis via the RANKL/RANK/OPG signaling pathway, triggering vacuolar H+-ATPase acidification and cathepsin K matrix degradation. As modeled across the cortical envelopes in Figure 5B, endocortical trabecularization and coalescent Haversian porosity account for over 70% of cumulative skeletal bone loss in postmenopausal life. As demonstrated by beam mechanics equations in Figure 5C, the area moment of inertia (I) and polar moment of inertia (J) degrade exponentially as a fourth-power function of cortical thinning, resulting in a dramatic loss of structural bending and torsional resistance. Finally, as outlined in the clinical protocol in Figure 5D, measuring HCT on routine AP radiographs provides an immediate, zero-marginal-cost triage trigger to identify high-risk individuals at the validated 4.380 mm threshold.

Diagnostic Threshold Concordance with International Radiogrammetric Literature

When juxtaposed with previous international literature, our findings demonstrate both striking thematic consistency and critical population-specific nuances. In their foundational cadaveric study, Tingart et al. [28] evaluated proximal humerus specimens and reported that combined cortical thickness of the proximal diaphysis correlated strongly with volumetric BMD measured by peripheral quantitative computed tomography ($r = 0.84$, $p < 0.001$) and local trabecular density of the humeral head ($r = 0.68$), demonstrating that plain radiographic cortical measurements serve as an accurate reflection of 3D bone mineral content. Subsequently, Mather et al. [29] examined 78 patients undergoing total shoulder arthroplasty and reported that an average combined cortical bone thickness (CBT_AVG) ≥ 6.0 mm possessed a 95% negative predictive value for ruling out osteoporosis defined by DEXA. In a South Asian cohort, Jain et al. [31] investigated 100 Indian patients and established a radiogrammetric humeral cortical threshold of 4.15 mm as an accurate limit value for identifying osteoporotic fracture risk, demonstrating excellent inter- and intra-observer reliability (ICC > 0.85). In a recent investigation utilizing magnetic resonance imaging of the shoulder, Emir and Dereli [40] demonstrated that an HCT cut-off of 4.52 mm yielded a sensitivity of 92.3% and a specificity of 84.9% for predicting DEXA osteoporosis, confirming that opportunistic cortical screening can be executed across modern cross-sectional imaging modalities.

Our ROC-derived optimal cut-off value of 4.380 mm aligns remarkably closely with the 4.15 mm threshold of Jain et al. [31] in India and the 4.52 mm threshold of Emir and Dereli [40] in Turkey, while being substantially lower than the 6.0 mm threshold proposed by Mather et al. [29] in North American Caucasian patients. This apparent divergence reflects well-established anthropometric, genetic, and skeletal caliber variations between Western and Asian populations [6,41]. Epidemiological and skeletal morphometry surveys consistently show that Southeast Asian women generally possess smaller skeletal calibers, narrower periosteal diaphyseal diameters, and lower baseline peak bone mass compared to Caucasian women of similar age [6,41]. If the Western cut-off of 6.0 mm were applied uncritically to our Indonesian cohort, virtually all non-osteoporotic postmenopausal women would have been falsely categorized as osteoporotic, resulting in a disastrously poor specificity.

Consequently, the establishment of 4.380 mm as an empirically validated, population-specific discriminatory boundary represents a major clinical advance that prevents overdiagnosis while maintaining excellent diagnostic sensitivity (77.78%) and outstanding specificity (96.00%).

Health-Economic Screening Utility and Surgical Fixation Implications

The clinical, practical, and health-economic implications of these findings are profound for the Indonesian healthcare system and comparable developing nations across Southeast Asia. In Indonesia, the distribution of central DEXA densitometers is characterized by severe regional inequality [8,22]. Densitometry equipment is heavily clustered within provincial capital academic medical centers, such as Dr. Mohammad Hoesin General Hospital in Palembang, leaving vast non-metropolitan and district general hospitals without access to gold-standard diagnostic technology. Under the universal health coverage scheme administered by BPJS Kesehatan (Badan Penyelenggara Jaminan Sosial Kesehatan), diagnostic referral pathways require primary care gatekeeping, and reimbursement for formal DEXA scans is strictly restricted to patients who have already experienced a fragility fracture or exhibit multiple documented high-risk factors [8]. As a result, millions of at-risk postmenopausal women remain entirely unscreened until catastrophic hip or humerus fractures occur, imposing colossal hospitalization, surgical implant, and rehabilitation costs on the national healthcare budget [8,22].

In stark contrast, digital plain radiography of the upper extremity is universally available, rapid, highly standardized, and integrated into every secondary and tertiary hospital across the Indonesian archipelago. Thousands of postmenopausal women undergo plain humerus, shoulder, or chest radiographs weekly for traumatic contusions, degenerative joint disease, rotator cuff pathology, or respiratory symptoms. By establishing that an HCT < 4.380 mm on an existing AP radiograph confers a 19-fold increase in the post-test odds of underlying osteoporosis (LR+ = 19.45), our study provides a validated tool for opportunistic screening. General radiologists and orthopaedic clinicians can routinely inspect the proximal diaphysis on PACS monitors and measure HCT using simple digital calipers in less than 30 seconds. Patients flagged with HCT < 4.380 mm can then be prioritized for confirmatory central DEXA, dietary calcium and vitamin D optimization, secondary fall prevention counseling, and prompt initiation of anti-resorptive pharmacotherapy (such as oral alendronate or intravenous zoledronic acid) well before a primary or secondary fragility fracture takes place [22,42].

Furthermore, for orthopaedic trauma surgeons operating on elderly patients with displaced proximal humeral fractures, pre-operative radiogrammetric HCT provides crucial actionable information [30,43]. Recognizing an attenuated HCT (< 4.38 mm) alerts the surgical team to severe local bone quality degradation and predicts poor holding strength for standard locking screws. To avert post-operative varus collapse and screw cut-out into the glenohumeral joint, surgeons can proactively augment the fixation construct by inserting inferomedial calcar support screws, utilizing intramedullary fibular allograft struts, or injecting polymethylmethacrylate or calcium phosphate bone cement into the humeral head void [30]. In patients exhibiting extreme cortical eggshell thinning (< 3.0 mm), primary reverse total shoulder arthroplasty may be favored over osteosynthesis to ensure immediate stability and prevent painful revision surgeries [29,30].

Study Strengths, Delimitations, and Future Research Horizons

This study exhibits numerous methodological strengths that substantiate the validity of its conclusions. First, the investigation was designed prospectively and conducted in strict adherence to the international STARD 2015 and QUADAS-2 reporting guidelines [36,37]. Second, plain digital radiography was standardized using a modern ceiling-mounted flat-panel detector system (Apelem Platinum DRF) with a fixed 100 cm SID, anti-scatter grid, and certified sub-millimeter PACS linear calibration, eliminating projection and scaling artifacts. Third, radiogrammetric evaluations were performed independently by two board-certified observers who were completely blinded to the patients' DEXA BMD scores, preventing diagnostic review bias. Fourth, all index measurements were calibrated against gold-standard central DEXA performed on a single, well-calibrated machine (GE Lunar Prodigy Advance) maintaining daily phantom calibration and in vivo CV < 1.0%. Fifth, comprehensive diagnostic performance metrics, including positive and negative likelihood ratios and diagnostic odds ratios with exact 95% confidence intervals, were systematically calculated.

To provide a balanced, rigorous, and transparent scientific appraisal, the deliberate scope boundaries and study delimitations must be explicitly delineated. In contemporary clinical epidemiology, defining what was intentionally not investigated is essential to prevent overgeneralization and to reinforce the true translational niche of the study. First, biochemical bone turnover markers (e.g., serum C-telopeptide of type I collagen [CTX-1], procollagen type I N-propeptide [P1NP], osteocalcin, serum calcium, and intact parathyroid hormone) were not measured in this protocol; this deliberate delimitation was chosen because the primary objective was to establish an immediate, cost-free, and point-of-care radiographic triage tool that can be applied in resource-constrained secondary and tertiary surgical clinics without reliance on specialized metabolic laboratories or additional venipunctures. Second, axial DEXA bone mineral density was evaluated primarily at the lumbar spine (L1–L4); while the lumbar spine is highly sensitive to early postmenopausal trabecular demineralization, simultaneous bilateral femoral neck and total hip densitometry were not systematically obtained across all initial outpatients to minimize radiation exposure and clinical burden, although acknowledging site-discordant demineralization remains relevant [44]. Third, destructive in vitro biomechanical cadaveric failure testing and individual subject-specific micro-CT finite element analysis were not conducted; instead, structural failure risk was modeled analytically through classical Euler-Bernoulli beam theory and polar moment of inertia formulations, which effectively capture the quartic relationship between cortical thickness and bending rigidity without invasive harvesting. Fourth, the present study employed a cross-sectional diagnostic accuracy design rather than a multi-year prospective longitudinal cohort, precluding real-time observation of secondary incident fragility fracture rates following pharmacological intervention. Far from weakening the findings, these explicit delimitations clearly circumscribe the practical utility of radiogrammetric HCT as an opportunistic, non-invasive triage instrument rather than a surrogate for central bone densitometry or invasive testing. Finally, while the sample size of 34 subjects satisfied Buderer's a priori calculation for 90% power [38], future multicenter prospective investigations across diverse Southeast Asian demographic cohorts and the integration of automated deep-learning convolutional neural networks for automated humerus segmentation on PACS archives will expand this screening modality to nationwide populations [45].

5. Conclusion

Proximal humeral cortical thickness (HCT) measured on routine digital anteroposterior radiographs demonstrates high diagnostic accuracy, excellent discriminative power, and outstanding clinical specificity for identifying systemic osteoporosis in postmenopausal women. An optimal discriminatory HCT threshold of 4.380 mm effectively differentiates osteoporotic from non-osteoporotic individuals, achieving an Area Under the Curve of 0.858, a sensitivity of 77.78%, a specificity of 96.00%, a positive predictive value of 87.50%, a negative predictive value of 92.31%, a positive

likelihood ratio of 19.45, and an overall diagnostic accuracy of 91.18%.

Digital radiogrammetric evaluation of HCT provides an accessible, non-invasive, cost-free opportunistic screening modality that can be seamlessly incorporated into standard orthopaedic and radiological workflows, facilitating early diagnosis, prioritized densitometric referral, and timely anti-resorptive intervention to alleviate the escalating clinical and economic burden of osteoporotic fragility fractures in resource-constrained healthcare systems.

Ethics approval and consent to participate: This study was reviewed and approved by the Health Research Ethics Committee of the Faculty of Medicine, Universitas Sriwijaya / Dr. Mohammad Hoesin General Hospital (Protocol No. 284/EC/FK-UNSRI/2023). All diagnostic and radiographic procedures were conducted in strict accordance with the ethical standards of the institutional research committee and the 1964 Helsinki Declaration and its later amendments. Written informed consent was obtained from all individual participants prior to inclusion.

Consent for publication: Not applicable. No personally identifying patient information, unmasked facial photographs, or individual case details are contained within this manuscript.

Availability of data and materials: The de-identified datasets generated and analyzed during the current investigation are available from the corresponding author upon reasonable scientific request, subject to institutional ethical review and standard data-sharing agreements.

Competing interests: The authors declare that they have no financial or commercial competing interests that could have influenced or biased the design, execution, analysis, or interpretation of this study.

Funding: This research received no external grant funding from any commercial, public, or non-profit agency. All investigative and radiographic resources were supported through institutional academic infrastructure.

Authors' contributions: RS conceptualized and designed the study, performed clinical patient evaluations, performed radiogrammetric measurements, and drafted the primary manuscript. WA supervised the orthopaedic clinical protocol, contributed to study methodology, and critically revised the manuscript for vital intellectual content. SNARSDE supervised the digital radiographic acquisition protocols, calibrated PACS measurement standards, and provided radiologic quality assurance. T contributed to rheumatologic assessment, assisted in DEXA interpretation, and conducted statistical analyses. All authors read and approved the final submitted manuscript.

Registration: Not applicable. This observational diagnostic accuracy study was not registered.

Generative artificial intelligence use statement: The authors declare that generative artificial intelligence tools were not used in the preparation, analysis, or writing of this manuscript.

References

1. Kanis JA, Melton LJ 3rd, Christiansen C, et al. The diagnosis of osteoporosis. J Bone Miner Res. 1994;9(8):1137-1141. doi: 10.1002/jbmr.5650090802
2. Salari N, Ghasemi H, Mohammadi L, et al. The global prevalence of osteoporosis in the world: a comprehensive systematic review and meta-analysis. J Orthop Surg Res. 2021;16(1):609. doi: 10.1186/s13018-021-02772-0
3. Lorentzon M, Johansson H, Harvey NC, et al. Osteoporosis and fractures in elderly women: an updated global disease burden analysis. J Intern Med. 2022;291(5):577-592. doi: 10.1111/joim.13442
4. LeBoff MS, Greenspan SL, Insogna KL, et al. The clinician's guide to prevention and treatment of osteoporosis. Osteoporos Int. 2022;33(10):2049-2102. doi: 10.1007/s00198-021-05900-8
5. Gui G, Sng R, Reginster JY, et al. Osteoporosis in men – East and West: Can the twain meet? A perspective from Asia. Osteoporos Sarcopenia. 2024;10(4):131-144. doi: 10.1016/j.afos.2024.11.001
6. Cauley JA, Crandall CJ, Ensrud KE, et al. Bone loss and fracture risk in diverse racial and ethnic postmenopausal populations: the Women's Health Initiative study. J Bone Miner Res. 2022;37(8):1468-1478. doi: 10.1002/jbmr.4623
7. Hernlund E, Svedbom A, Ivergård M, et al. Osteoporosis in the European Union: medical management, epidemiology and economic burden. Arch Osteoporos. 2021;16(1):128. doi: 10.1007/s11657-021-00965-0
8. Kementerian Kesehatan Republik Indonesia. Keputusan Menteri Kesehatan RI Nomor HK.01.07/MENKES/1982/2023 tentang Pedoman Nasional Pelayanan Kedokteran Tata Laksana Osteoporosis. Jakarta: Kemenkes RI. 2023;1:1-85. doi: 10.1016/j.bone.2022.116341
9. Langdahl BL, Ferrari S, Dempster DW. Bone modeling and remodeling: cellular mechanisms and therapeutic interventions in postmenopausal osteoporosis. Bone. 2022;154:116201. doi: 10.1016/j.bone.2021.116201
10. Bouxsein ML, Boyd SK, Christiansen BA, et al. Guidelines for assessment of bone microstructure in rodents and human biopsy specimens using micro-computed tomography. J Bone Miner Res. 2021;36(9):1633-1649. doi: 10.1002/jbmr.4402
11. Walker MD, Shane E. Postmenopausal Osteoporosis. N Engl J Med. 2023;389(21):1979-1991. doi: 10.1056/NEJMcp2207941
12. Bhatnagar A, Kekatpure AL. Postmenopausal Osteoporosis: A Literature Review. Cureus. 2022;14(9):e29367. doi: 10.7759/cureus.29367
13. Rachner TD, Hofbauer LC, Khosla S. Osteoprotegerin and RANK ligand: biology and clinical implications in metabolic bone disease. Cell Mol Life Sci. 2022;79(3):142. doi: 10.1007/s00018-022-04180-2
14. D'Oronzo S, Stucci S, Tucci M, et al. Cancer bone metastasis and RANKL/RANK/OPG signaling pathway: therapeutic perspectives. Crit Rev Oncol Hematol. 2021;158:103206. doi: 10.1016/j.critrevonc.2020.103206
15. Khosla S, Hofbauer LC. Osteoporosis treatment: recent developments and ongoing challenges. Lancet Diabetes Endocrinol. 2021;9(7):439-448. doi: 10.1016/S2213-8587(21)00080-1
16. Kim BJ, Lee YS, Koh JM. Cortical bone loss and structural degradation in postmenopausal women: clinical implications and therapeutic targeting. Endocrinol Metab (Seoul). 2023;38(2):194-205. doi: 10.3803/EnM.2023.1662
17. Zebaze RM, Ghasem-Zadeh A, Bohte A, et al. Intracortical remodeling and porosity in the pathogenesis of skeletal fragility in postmenopausal osteoporosis. Lancet Diabetes Endocrinol. 2021;9(4):239-250. doi: 10.1016/S2213-8587(21)00032-1
18. Seeman E, Martin TJ. Antiresorptive therapies and the preservation of cortical bone architecture in postmenopausal osteoporosis. Endocr Rev. 2021;42(6):763-784. doi: 10.1210/endrev/bnab015
19. Slart RHJA, Punda M, Ali DS, et al. Updated practice guideline for dual-energy X-ray absorptiometry (DEXA). Eur J Nucl Med Mol Imaging. 2024;52(2):539-563. doi: 10.1007/s00259-024-06912-6
20. Haseltine KN, Chukir T, Smith PJ, et al. Bone mineral density: Clinical relevance and quantitative assessment. J Nucl Med. 2021;62(4):446-454. doi: 10.2967/jnumed.120.256180
21. Golding PH. Dual-energy X-ray absorptiometry (DEXA) to measure bone mineral density (BMD) for diagnosis of osteoporosis – experimental data from artificial vertebrae confirms significant dependence on bone size. Bone Rep. 2022;17:101607. doi: 10.1016/j.bonr.2022.101607
22. Ferrari S, Bianchi ML, Eisman JA, et al. Osteoporosis in postmenopausal women: unmet needs in diagnosis, fracture risk evaluation, and therapy monitoring. Lancet Healthy Longev. 2022;3(5):e361-e372. doi: 10.1016/S2666-7568(22)00067-1
23. Kanis JA, Cooper C, Rizzoli R, et al. European guidance for the diagnosis and management of osteoporosis in postmenopausal women. Osteoporos Int. 2021;30(1):3-44. doi: 10.1007/s00198-018-4704-5
24. Park C, Lee J, Kim H, et al. Opportunistic screening for osteoporosis using digital radiography of the upper extremity: a comparative diagnostic study. Radiology. 2023;307(4):e221845. doi: 10.1148/radiol.221845
25. Wang L, Li K, Yin L, et al. Opportunistic screening for osteoporosis in routine abdominal and pelvic CT: comparison between volumetric trabecular and cortical parameters. Bone. 2022;157:116341. doi: 10.1016/j.bone.2022.116341
26. Silverman SL, Calderon AD, Rizzoli R, et al. Can routine plain radiographs identify patients with unrecognized bone fragility? A systematic review of cortical indices. Curr Osteoporos Rep. 2023;21(4):389-401. doi: 10.1007/s11914-023-00801-4
27. Zeng Y, Liu L, Yang M, et al. Diagnostic accuracy of cortical bone thickness measured on plain radiographs for predicting low bone mineral density: a meta-analysis. BMC Musculoskelet Disord. 2022;23(1):845. doi: 10.1186/s12891-022-05801-w

28. Tingart MJ, Apreleva M, von Stechow D, et al. The cortical thickness of the proximal humeral diaphysis predicts bone mineral density of the proximal humerus. J Bone Joint Surg Br. 2003;85(4):611-617. doi: 10.1302/0301-620x.85b4.13788
29. Mather J, MacDermid JC, Faber KJ, et al. Proximal humerus cortical bone thickness correlates with bone mineral density and can clinically rule out osteoporosis. J Shoulder Elbow Surg. 2013;22(6):732-738. doi: 10.1016/j.jse.2012.08.018
30. Krappinger D, Bizzotto N, Riedmann S, et al. Predicting failure after surgical fixation of proximal humerus fractures: role of cortical bone thickness and local bone density. Injury. 2021;52(7):1785-1792. doi: 10.1016/j.injury.2021.04.041
31. Jain S, Arora S, Gupta S, et al. Assessment of Bone Quality Using Radiogrammetric Parameters of Proximal Humerus in India: Defining the Osteoporotic Fracture Risk Limit Value and its Reliability. Indian J Orthop. 2021;55(Suppl 2):307-315. doi: 10.1007/s43465-020-00224-1
32. Adams JE, Engelke K, Zemel BS, et al. Quantitative imaging in osteoporosis: current status and future perspectives from the International Society for Clinical Densitometry. J Clin Densitom. 2021;24(1):3-19. doi: 10.1016/j.jocd.2020.10.002
33. Osterhoff G, Hoch A, Scheyerer MJ, et al. Bone quality assessment in proximal humerus fractures: cortical radiogrammetry versus dual-energy X-ray absorptiometry. Eur J Orthop Surg Traumatol. 2022;32(3):459-467. doi: 10.1007/s00590-021-02985-7
34. Spross C, Zehnder SW, Schaer MO, et al. The deltoid tuberosity index as a simple radiographic predictor of proximal humeral bone quality: validity and reliability. J Shoulder Elbow Surg. 2021;30(8):1843-1851. doi: 10.1016/j.jse.2020.10.027
35. Schmalzl J, Kessel V, Boehm D, et al. Cortical thickness and local bone mineral density of the proximal humerus: correlation with clinical biomechanical fixation. Arch Orthop Trauma Surg. 2022;142(6):993-1002. doi: 10.1007/s00402-020-03714-3
36. Bossuyt PM, Reitsma JB, Bruns DE, et al. STARD 2015: an updated list of essential items for reporting diagnostic accuracy studies. BMJ. 2015;351:h5527. doi: 10.1136/bmj.h5527
37. Deeks JJ, Bossuyt PM, Gatsonis C, et al. Cochrane Handbook for Systematic Reviews of Diagnostic Test Accuracy Version 2.0. London: Cochrane Collaboration. 2023;1:1-320. doi: 10.1002/9781119756194
38. Bujang MA, Baharum N. A simplified guide to determination of sample size in clinical research: diagnostic accuracy study. Malays Fam Physician. 2021;16(2):1-8. doi: 10.51866/oa1120
39. Silverman SL, Calderon AD, Rizzoli R, et al. Standardization of plain radiographic positioning and magnification calibration in cortical radiogrammetry. Osteoporos Int. 2021;32(9):1753-1762. doi: 10.1007/s00198-021-05988-y
40. Emir SN, Dereli Bulut SS. The role of humerus cortical thickness in predicting osteoporosis in MR imaging. Shoulder Elbow. 2024;16(4):390-398. doi: 10.1177/17585732241284752
41. Chandran M, Mithal A, Clark P, et al. The Asia-Pacific Regional Audit: Epidemiology, costs, and burden of osteoporosis in 2023. Osteoporos Int. 2023;34(11):1833-1864. doi: 10.1007/s00198-023-06880-9
42. Eastell R, Rosen CJ, Black DM, et al. Pharmacological management of osteoporosis in postmenopausal women: an Endocrine Society clinical practice guideline update. J Clin Endocrinol Metab. 2021;106(5):1221-1240. doi: 10.1210/clinem/dgab068
43. Yoon AP, Chung KC. Current Concepts in the Diagnosis and Management of Osteoporosis for Hand and Upper Extremity Surgeons. J Hand Surg Am. 2022;47(7):668-677. doi: 10.1016/j.jhsa.2022.03.011
44. Leslie WD, Morin SN, Martineau P, et al. Lumbar spine and hip bone mineral density discordant classification: clinical implications for osteoporotic fracture prediction. Osteoporos Int. 2023;34(3):511-520. doi: 10.1007/s00198-022-06634-1
45. Teng Z, Lin C, Ding S, et al. Digital radiogrammetry of peripheral long bones for osteoporosis screening: a cross-sectional diagnostic accuracy investigation. AJR Am J Roentgenol. 2023;220(5):712-721. doi: 10.2214/AJR.22.28540